

Mechanical Response and Microprocesses of Reconsolidating Crushed Salt at Elevated Temperature

S. T. Broome¹ · S. J. Bauer¹ · F. D. Hansen² · M. M. Mills³

Received: 31 August 2015 / Accepted: 1 September 2015 / Published online: 14 September 2015
© Springer-Verlag Wien (outside the USA) 2015

Abstract Design, analysis and performance assessment of potential salt repositories for heat-generating nuclear waste require knowledge of thermal, mechanical, and fluid transport properties of reconsolidating granular salt. To inform salt repository evaluations, we have undertaken an experimental program to determine Bulk and Young's moduli and Poisson's ratio of reconsolidated granular salt as a function of porosity and temperature and to establish the deformational processes by which the salt reconsolidates. Tests were conducted at 100, 175, and 250 °C. In hydrostatic tests, confining pressure is increased to 20 MPa with periodic unload/reload loops to determine K . Volume strain increases with increasing temperature. In shear tests at 2.5 and 5 MPa confining pressure, after confining pressure is applied, the crushed salt is subjected to a differential stress, with periodic unload/reload loops to determine E and ν . At predetermined differential stress levels the stress is held constant and the salt consolidates. Displacement gages mounted on the samples show little lateral deformation until the samples reach a porosity of ~ 10 %. Interestingly, vapor is vented only for 250 °C tests and condenses at the vent port. It is hypothesized that the brine originates from fluid inclusions, which were made accessible by heating and intragranular deformational processes including decrepitation. Identification and documentation

of consolidation processes are inferred from optical and scanning electron microstructural observations. Densification at low porosity is enhanced by water film on grain boundaries that enables solution-precipitation phenomena.

Keywords Crushed salt reconsolidation · Mechanical testing · High temperature · Hydrostatic · Triaxial · Salt creep · Elastic properties

1 Introduction

Understanding and predicting the reconsolidation behavior of granular crushed salt is vital to backfilling or sealing nuclear waste repositories in salt. Significant research efforts have attempted to address this recognized need resulting in a long history of crushed salt backfill testing for salt repository applications. Callahan (1999) summarized the constitutive model for room temperature consolidation with application to the shaft seal system at the Waste isolation pilot plant (WIPP). Over the years, salt reconsolidation has been a topic of great interest to international salt repository studies as exemplified by recurring symposia (for example: Aubertin and Hardy 1996; Wallner et al. 2007). A preponderance of these studies focused on room temperature experiments, with only a few tests conducted at elevated temperatures up to 100 °C. Today there is a renewed national and international interest in salt reconsolidation at elevated temperature, particularly as applied to disposal of heat-generating nuclear waste.

In recognition of the need for this essential research, the United States (US) Department of Energy supported investigations to explore and solidify our understanding of reconsolidation of granular salt under high temperatures. For this purpose, a new experimental procedure for a

✉ S. T. Broome
stbroom@sandia.gov

¹ Geomechanics Department, Sandia National Laboratory, Albuquerque, NM, USA

² Geoscience Research and Applications, Sandia National Laboratories, Albuquerque, NM, USA

³ Nuclear Waste Disposal Research and Analysis, Sandia National Laboratories, Albuquerque, NM, USA

laboratory study of reconsolidation of salt aggregate was developed, emphasizing testing at elevated temperature. Successful completion of these experiments under challenging pressure and temperature regimes required development of advanced geomechanics experimental techniques.

The salt used in these experiments is called “run-of-mine” which means the aggregate was produced during normal mining operations at WIPP (with aggregate pieces greater than 9.5 mm removed). The laboratory studies provide data representing consolidation behavior as a function of stress state and temperatures up to 250 °C.

The laboratory test procedures used both hydrostatic (isostatic) and shear stresses to consolidate the mine-run salt. Hydrostatic refers to the application of a uniform or isotropic stress state, while shear stresses involve the superposition of an additional axial stress. Consolidation under shear stress more realistically represents conditions expected in a disposal concept where hydrostatic stress conditions are unlikely for early times and the roof-to-floor closure would be faster than the rib-to-rib closure.

In addition to elevated temperature, hydrostatic pressures up to 20 megapascal (MPa) and stress differences up to 10 MPa were applied. The stresses correspond to in situ stresses encountered at commercial salt mining operations as well as WIPP.

It was initially thought that the effective pressure-solution re-deposition process would be minimized because available and accessible brine would be driven off by high temperatures and venting of the samples. Further, it was hypothesized that the intragranular fluid inclusions within the crystal structure would remain trapped. As will be discussed later in this paper, neither hypotheses proved correct, which are key findings of this research. Drying may occur with an accompanying change of consolidation mechanisms; this is a potentially important hypothesis relevant to crushed salt in a heat-generating salt repository. Such experimental work was identified to be of great interest to national and international salt repository programs (Hansen and Leigh 2011).

2 Background and Techniques

A suite of experiments was designed to systematically evaluate the consolidation of crushed salt as a function of stress (σ) and temperature (T) conditions. Laboratory studies provide consolidation behavior for temperature to 250 °C and mean stress to 20 MPa.

The test matrix is summarized in Table 1, which lists the test type, stress, temperature conditions, and other test information. Three test types used in this test series are isostatic, shear and shear in combination with creep of

right-circular cylindrical specimens. Most of the tests had multiple stages, for example, an initial isostatic segment followed by one or more shears and creep consolidation portions. The sequence and type of experimental test conditions of temperature, pressure, and shear were chosen to allow parameterization of appropriate constitutive models using a minimum number of tests.

For all tests, jacketed specimens of crushed mine-run salt from the WIPP were dried at 105 °C until no further weight loss occurred. Undeformed right-circular cylindrical specimen assemblies of unconsolidated granular salt with initial porosities of $\sim 40\%$, nominally 10 cm in diameter and 17.5 cm in length, were jacketed in malleable soldered lead tubes. Samples were placed in a pressure vessel and kept at test temperatures of 100, 175 or 250 °C and vented to the atmosphere during the entire test procedure.

In isostatic tests, confining pressure is slowly increased at pressurization rates ranging from ~ 0.0005 MPa/s at the beginning of the test to ~ 0.0422 MPa/s near the end by pumping silicon oil confining fluid at rates of 9.46 mL/min or by advancing the actuator at a rate of 0.00254 cm/s into the pressure vessel (both pressurization methods increased pressure at equivalent but non-uniform rates). During pressurization, pressure and sample displacement (used to determine strain) are recorded. Also, at predetermined pressure levels, pressurization is reversed to 1/3–1/2 the previous maximum level, then loading is resumed. This is termed an unload/reload loop; from such a loop the bulk modulus may be determined.

In shear tests, after an isostatic pressure increase to a predetermined level, the axial piston housed in the loading frame is advanced in a quasistatic manner (an actuator displacement rate of 0.00127 cm/s is equivalent to $\sim 8 \times 10^{-5}$ /s strain rate on a 15.49 cm long sample) until a predetermined stress level (Table 1) is attained. At predetermined axial stress levels, axial loading is reversed to 1/3–1/2 the starting differential stress level, then loading is resumed. In this type of unload/reload loop, the elastic Young’s modulus and Poisson’s ratio may be determined. The specimen is typically held at constant differential stress and allowed to creep until approximately 5 % additional axial strain accrues through creep consolidation. At that point, the axial piston is advanced in a quasistatic manner until the second predetermined stress level (Table 1) is attained (accompanied by unload/reload loops during loading). The specimen is allowed to creep (and further consolidate) at the higher stress level until approximately 5 % additional axial strain is experienced. Then the axial load is reduced to zero, the confining pressure is reduced to zero, and the heating elements are turned off allowing the specimen to cool to ambient temperature.

Table 1 Test Matrix for Salt Reconsolidation at Elevated Temperature

Test number	Test type	T (°C)	Maximum confining pressure ^a (MPa)	Axial stress ^b (MPa)	Mean stress (MPa)	Stress difference (MPa)	Description ^c	Comment
1	Isostatic	100	2.5	2.5	2.5	0.0	Quasistatic	Phase 1 of Test 16
2	Isostatic	100	5.0	5.0	5.0	0.0	Quasistatic	Phase 1 of Test 17
3	Isostatic	175	2.5	2.5	2.5	0.0	Quasistatic	Phase 1 of Test 18
4	Isostatic	175	5.0	5.0	5.0	0.0	Quasistatic	Phase 1 of Test 19
5	Isostatic	250	2.5	2.5	2.5	0.0	Quasistatic	Phase 1 of Test 20
6	Isostatic	250	5.0	5.0	5.0	0.0	Quasistatic	Phase 1 of Test 21
7	Isostatic	250	20.0	20.0	20.0	0.0	Quasistatic	
8	Isostatic	250	10.0	10.0	10.0	0.0	Quasistatic	Phase 1 of Test 9
9	Shear	250	10.0	20.0	13.33	10.0	Quasistatic	Phase 2 of Test 8
10	Shear	100	2.5	5.0/7.5	3.33/4.17	2.50/5.0	Quasistatic	Phase 2 of Test 16
11	Shear	100	5.0	7.5/10.0	5.83/6.67	2.50/5.0	Quasistatic	Phase 2 of Test 17
12	Shear	175	2.5	5.0/7.5	3.33/4.17	2.50/5.0	Quasistatic	Phase 2 of Test 18
13	Shear	175	5.0	7.5/10.0	5.83/6.67	2.50/5.0	Quasistatic	Phase 2 of Test 19
14	Shear	250	2.5	5.0/7.5	3.33/4.17	2.50/5.0	Quasistatic	Phase 2 of Test 20
15	Shear	250	5.0	7.5/10.0	5.83/6.67	2.50/5.0	Quasistatic	Phase 2 of Test 21
16	Shear	100	2.5	5.0/7.5	3.33/4.17	2.50/5.0	Creep	Phase 3 of Tests 1 & 10
17	Shear	100	5.0	7.5/10.0	5.83/6.67	2.50/5.0	Creep	Phase 3 of Tests 2 & 11
18	Shear	175	2.5	5.0/7.5	3.33/4.17	2.50/5.0	Creep	Phase 3 of Tests 3 & 12
19	Shear	175	5.0	7.5/10.0	5.83/6.67	2.50/5.0	Creep	Phase 3 of Tests 4 & 13
20	Shear	250	2.5	5.0/7.5	3.33/4.17	2.50/5.0	Creep	Phase 3 of Tests 5 & 14
21	Shear	250	5.0	7.5/10.0	5.83/6.67	2.50/5.0	Creep	Phase 3 of Tests 6 & 15

T temperature

^a For quasistatic tests, stresses are increased from zero to the prescribed value with periodic unload/reload cycles for elastic property determination. The axial stress value is the same as the confining pressure value in the isostatic tests and greater than the confining pressure in the shear tests

^b For the shear loaded creep tests, both axial stress differences ($\Delta\sigma = 2.5$ and 5.0 MPa) will be run at the lower temperature values, but only the lower stress difference may be run at the higher temperatures depending on the prior results

^c The term “quasistatic” is used to describe tests wherein stresses are applied rapidly to minimize time-dependent effects. The term “creep” is used to describe tests wherein stresses are held constant at the prescribed test conditions for the duration of the test

The specimen assembly (Fig. 1) consists of a right-circular cylinder of unconsolidated granular salt, nominally 10 cm in diameter and 17.5 cm in length, constrained vertically between specially machined aluminum end caps. The machining of the outer diameter of the end caps enables a metal–metal seal of an outer lead jacket to the end cap. The upper end cap is vented to the atmosphere during the test to prevent buildup of vapor pore pressure. Beveled face plates are placed between the end caps and salt to accommodate the diameter change for the unconsolidated salt portion of the assembly and allow space for the inner lead jacket. A porous metal frit, shown in the figure as porous felt metal, is placed below the top end cap to allow fluid migration and venting across the entire specimen top surface area. The outer lead jacket, a soldered lead tube, laterally contains the entire assemble from top to

bottom, and isolates the inner lead jacket and the end caps from the confining medium. The lead is highly malleable and conforms to the shape of the specimen when hydrostatic pressure is applied.

Each assembly is fitted with two high temperature lateral deformation gages (Fig. 2) affixed near the specimen mid-height and oriented approximately orthogonal to one another. The specimen is placed in the pressure vessel (Fig. 3) by lowering the vessel over the specimen assembly. (Fig. 3 shows a specimen upon test completion below the pressure vessel.) The pressure vessel is then filled with confining fluid, heated to the test temperature at about 1 °C/min to minimize temperature gradients and allow uniform thermal expansion of the unconstrained specimen, and held at test temperature overnight at ambient pressure. At the initiation of the loading portion of the test, the

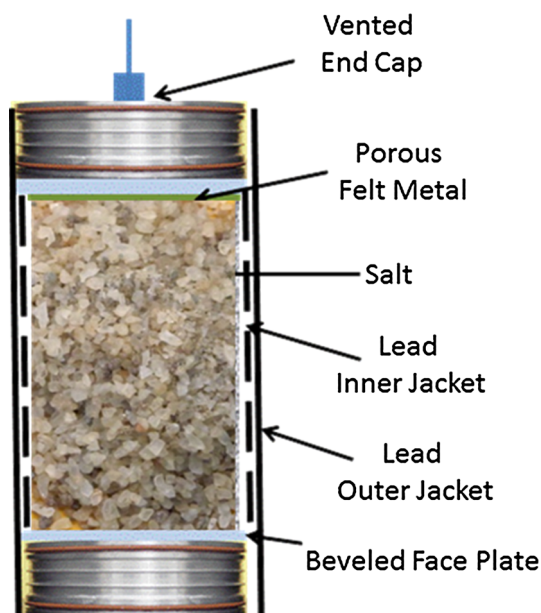


Fig. 1 Schematic of test arrangement



Fig. 2 Instrumented pretest specimen assembly

isostatic pressure is increased as described above, followed by the axial force/stress being increased as described above for the shear/creep portion of the test. A reconsolidated specimen in posttest condition is shown in Fig. 4. Note the significant dimpling of the lead jacket, caused by the



Fig. 3 Test apparatus with reconsolidated sample



Fig. 4 Specimen post test

presence of local voids and undulations in the granulated salt surface coupled with malleability of the lead jacketing material.

Jacket leaks were problematic at 250 °C because of extreme consolidation, large volumetric strains, and further softening of the lead jackets. To successfully mitigate the potential for jacket puncture, an intermediate thin copper sheet was placed between lead jackets for 250 °C tests as shown in Fig. 5a, b.

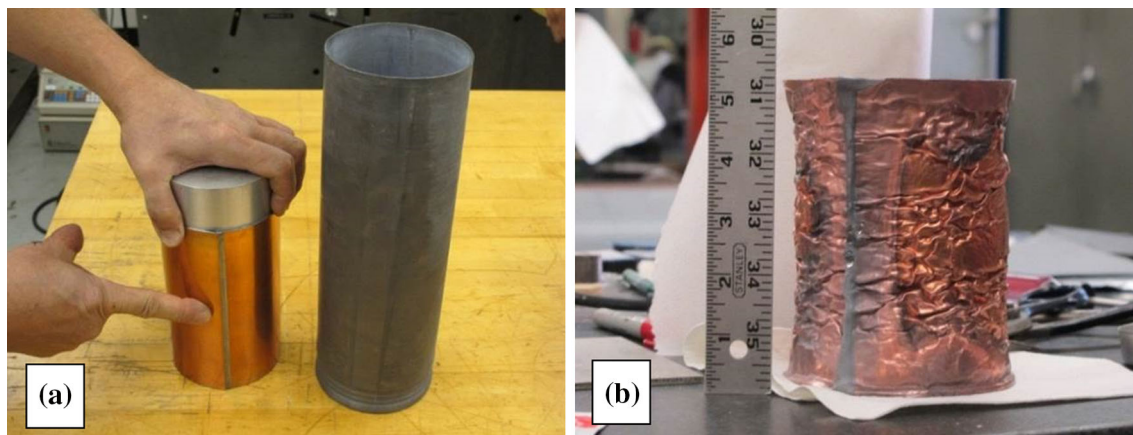


Fig. 5 **a** Application of copper jacket and **b** Copper jacket after 250 °C test

3 Results and Analysis

Table 2 provides a list of all laboratory tests completed and shows the correspondence of each test with the experimental matrix shown in Table 1. The experiments are identified with a unique identification number; the total volume strain, normalized density, and confining pressure are presented. The last column in Table 2 lists what tests were satisfied from Table 1. For example, if an Isostatic test went to 20 MPa confining pressure at 100 °C then all tests listed in Table 1 at or below 20 MPa confining pressure and at 100 °C were satisfied.

A significant, perhaps unexpected observation during these tests was the production of brine from the pore pressure port during 250 °C tests (Fig. 6). This occurred during the heating phase of these tests, when the specimen was unconfined. From Bauer et al. (2014), the expected weight percent brine loss at 100 °C is 0.10, at 175 °C 0.16, and at 250 °C 0.25. Further discussion of this observation is presented in Sect. 4.3.

3.1 Isostatic Tests

After the test temperature had stabilized overnight, confining pressure was increased to 20 MPa and specimen volume change was recorded either through dilatometry or using “on specimen” gages. At all temperatures, the specimens consolidate irreversibly with increasing pressure; the compacting specimen stiffens with increasing pressure. This is clearly shown in Fig. 7 where volume strain is compared to applied hydrostatic pressure for three tests at successively greater temperatures. As shown, increasing temperature facilitates compaction; i.e. more compaction is observed at a given pressure for greater temperatures. As the crushed salt is forced to compact, its

density increases (Fig. 8). The normalized density is the calculated density during the test divided by the theoretical density of solid salt (2.165 g/cc). The tests shown in Figs. 7 and 8 are FCT-CS-HQ-100-02, FCT-CS-HQ-175-01, and FCT-CS-HQ-250-02 from Table 2.

From the unload/reload loops in Figs. 7 and 8, it is visually obvious for the 250 °C test that the loops are not perfectly elastic. To further investigate this observation, the data from Figs. 7 and 8 are plotted in Fig. 9 in stress and strain versus time space.

While it is difficult to discern in Fig. 9 how strain behavior relates to stress behavior when observing the entire test, zoomed in unload/reload loops for each temperature at the same confining stress shown in Fig. 10 reveal that sample creep becomes more prevalent as temperature increases.

The unload reload loops conducted during the isostatic stage of each test facilitate determinations of the bulk modulus (K) at intervals during the deformation. In Fig. 11, K is plotted against normalized density for tests FCT-CS-HQ-ALL-01 and FCT-CS-CR-ALL-02. The “ALL” within the Sample ID indicates that the samples were compacted at more than one temperature. These tests had lateral deformation gages (as shown in Figs. 2, 3) affixed near sample mid-height. Volume strain was determined using these gages. Initially K is low and insensitive to an increase in normalized density until a normalized density of 0.75 is attained. Near this value of normalized density, K begins increasing with increasing normalized density to the maximum level observed. These data imply that K is primarily dependent on normalized density and less dependent on temperature. The maximal values of K 's are greater than the K of intact salt, which is a recognized and unresolved issue. The unreasonable calculated values are perhaps the result of the new experimental technique

Table 2 Summary of Tests Completed

Sample ID	Total Volumetric strain ε_V (%)	Normalized Density (% of theoretical)	Isostatic Confining pressure obtained (MPa)	Tests satisfied from test matrix (Table 1)
FCT-CS-HQ-100-02	28	79	20	1,2
FCT-CS-HQ-250-01	29, leak	78, leak	5.5	5,6
FCT-CS-HQ-175-01	35	87	16.6	3,4
FCT-CS-HQ-175-02				Actuator piston contacted sample at $\sigma_C = 10.3$ MPa
FCT-CS-HQ-250-02	37	93	20	5,6,7,8
FCT-CS-SQ-250-01	31, σ_C^a	84, σ_C^a	10	8
FCT-CS-SQ-250-02	37	93	10	9
FCT-CS-CR-250-01	33	86	2.5	14,20
FCT-CS-CR-250-02				
FCT-CS-CR-250-03				N/A (breach of confining medium into sample)
FCT-CS-CR-250-04				
FCT-CS-CR-175-01	31	86	2.5	12,18
FCT-CS-CR-175-02	32	85	5	13,19
FCT-CS-CR-100-01	19	73	2.5	10,16 ($\sigma_D = 2.5$ MPa only)
FCT-CS-CR-250-05	40	94	5	15,21
FCT-CS-CR-100-02	26	77	2.5	10,16
FCT-CS-CR-100-03	33	86	5	11,17
FCT-CS-CR-175-03	N/A ^b	N/A ^b	2.5	12,18 ($\sigma_D = 5$ MPa only)
FCT-CS-HQ-ALL-01	39	97	20	1,2
FCT-CS-CR-ALL-02	35	90	20	3,4

^a Values obtained after hydrostatic compaction are not available after the shear stage

^b Data not available at this time

developed during the test series. Also, the rate of unloading/reloading affected the data obtained, and subsequent calculation because the crushed salt was compacting during the course of the unload reload cycles as illustrated in Fig. 10. Additional data would improve our confidence in the experimental relationships developed.

3.2 Multistage Hydrostatic and Shear (Quasistatic and Creep) Tests

In this section examples of data from multistage tests are presented. After application of hydrostatic confining pressure, axial stress was increased in a quasistatic manner



Fig. 6 Brine exiting the pore pressure port at 250 °C

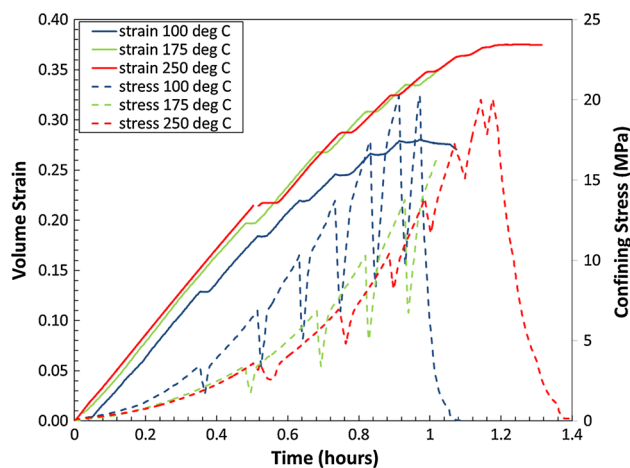


Fig. 9 Volume strain and hydrostatic confining pressure (σ_3) versus time

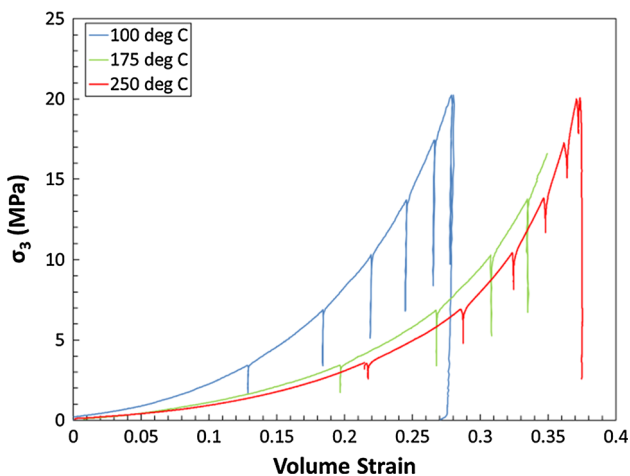


Fig. 7 Volume strain versus hydrostatic confining pressure (σ_3)

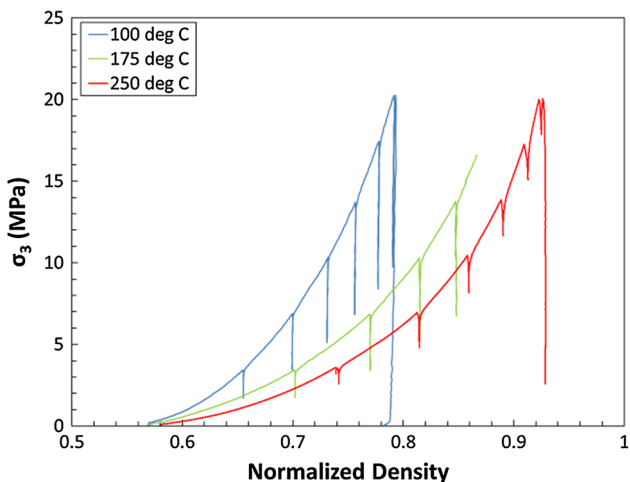


Fig. 8 Normalized density versus hydrostatic confining pressure (σ_3)

(slowly). Axial and radial displacement was measured for each specimen as a function of time. This allowed axial, lateral, and volume strain to be determined. Figure 12 shows a lateral strain versus hydrostatic confining pressure record from a 250 °C test. As confining pressure increases, the crushed salt compacts. In all tests, pressure was held constant for a brief time while preparing to apply axial force. This resulted in a small amount of isostatic creep compaction, about 1 % in this test.

In Fig. 13, the detailed stress–strain response for the differential stress portion of this 250 °C test is presented. During the initial axial loading, unload/reload loops are evident; as indicated, elastic moduli and Poisson’s ratio are deduced from the axial and lateral strains measured during this portion of the test. This is accomplished through fitting of the unload/reload loops with a best fit line. The zoom view provides insight into data quality, quantity, and fidelity. Upon reaching the creep stress, stress levels are held constant. True strains as opposed to engineering strains are used due to the large deformations.

Figure 14 presents a comparison of true strain (axial, lateral, and volume) for the three test temperatures. The strain–time response elucidates the temperature effect upon compaction in shear deformation, since the confining pressure (2.5 MPa) and differential stresses (2.5, 5.0 MPa) are the same for each temperature. The 100 °C test ran for about five days and is missing some early data due to a data logger malfunction, the 175 °C test ran for 13 h, and the 250 °C test ran for about 3 h. The density at the start of the shear portion of the test increased with increasing test temperature due to a greater amount of volume strain during the hydrostatic portion of the test. And, although the starting density is greatest for the 250 °C sample, it experiences the greatest axial and lateral strain at these

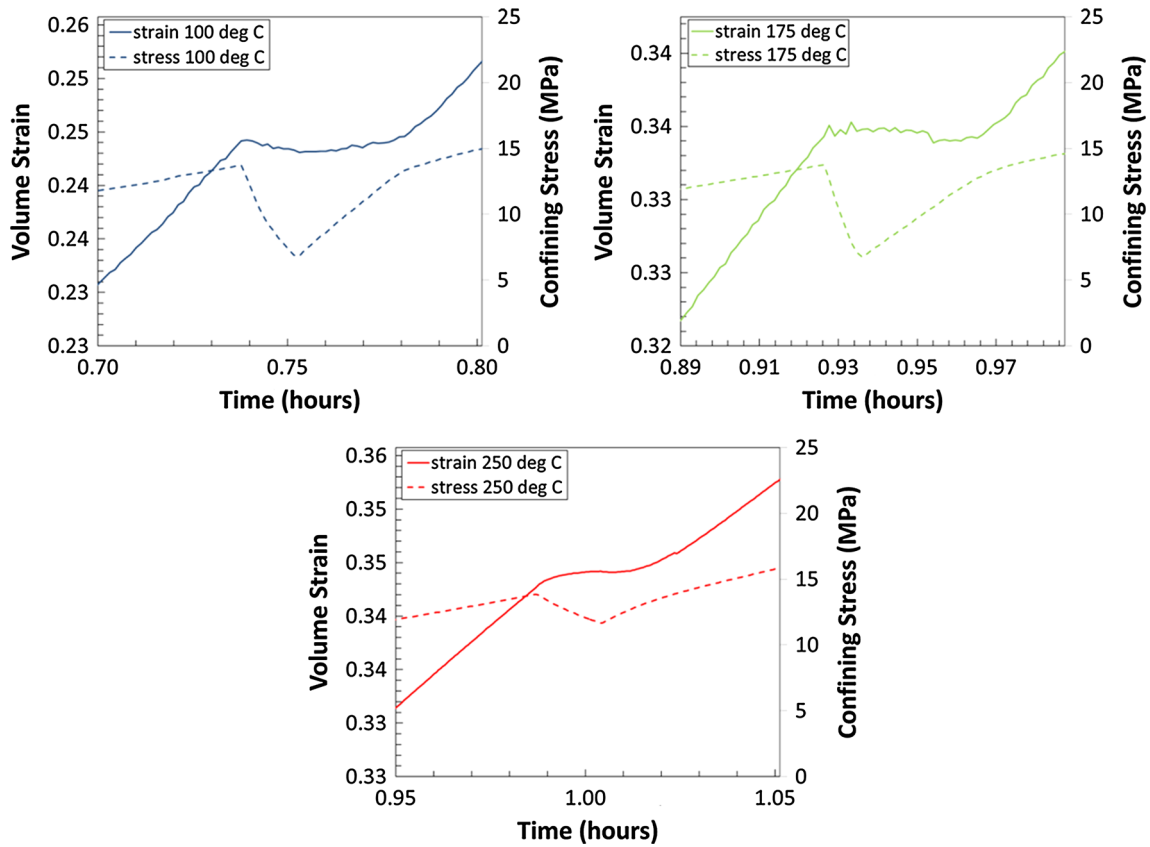


Fig. 10 Volume strain and hydrostatic confining pressure (σ_3) versus time showing detail of unload/reload loops at each temperature

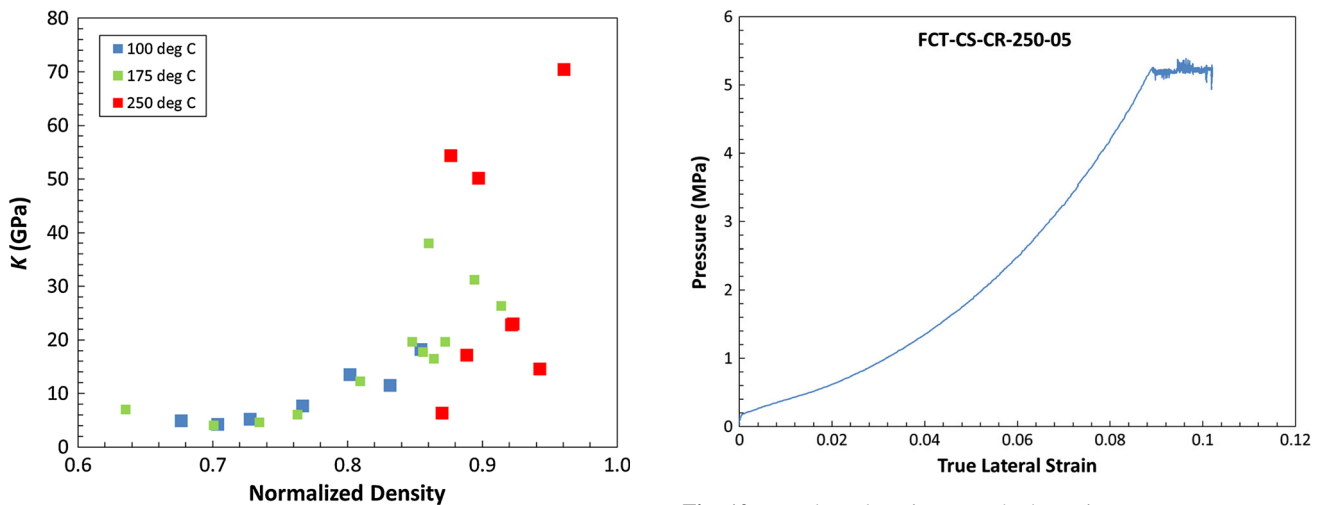


Fig. 11 Normalized density versus bulk modulus, K

Fig. 12 True lateral strain versus hydrostatic pressure

differential stresses, the strains for the 175 °C are intermediate, and the 100 °C sample experiences the smallest strains. The opposite trend is observed for volume strain. It is hypothesized that this is due to greater compaction during the hydrostatic portion of the test resulting in greater lateral strain during the shear portion of the test, the higher

the test temperature the less volume strain observed during the shear portion of the test.

The unload/reload loops during shear tests are used to determine Young’s modulus during the deformation. In Fig. 15, normalized Young’s modulus is plotted against normalized density. Young’s modulus appears to increase consistently with increasing normalized density at a given

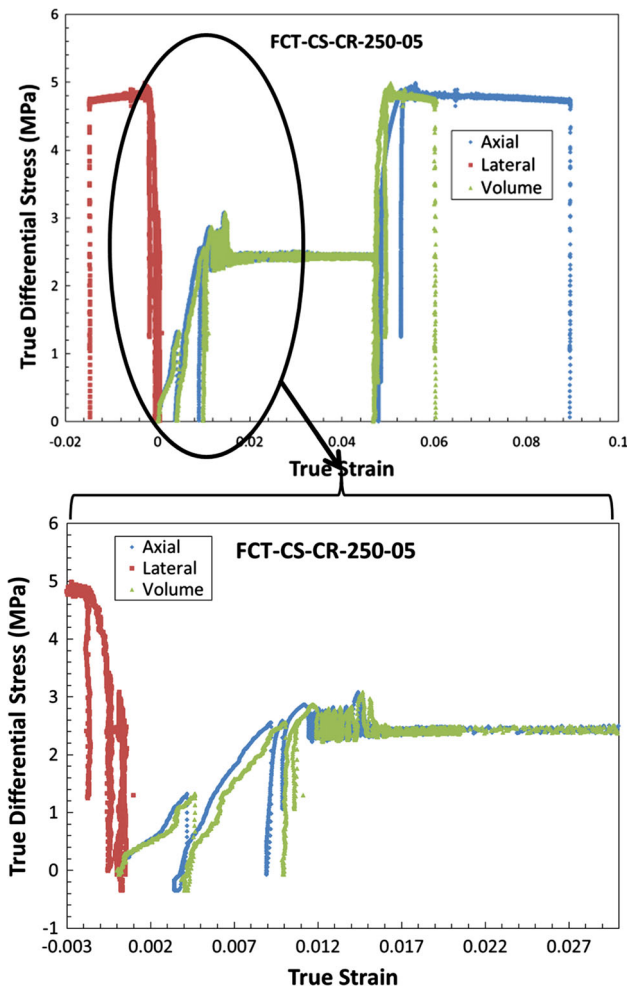


Fig. 13 Stress-strain response for a typical 250 °C test

temperature. Also, the data suggest that Young’s modulus decreases with increasing temperature; however, the data are too sparse to make definitive statements about the empirical relationships presented. The unload/reload loops were dependent on unload and reload rates because the porous salt aggregate was always creeping; the combination of experimental technique and ongoing deformation gave rise to the data scatter observed. Young’s modulus was normalized based on experimental data for intact WIPP salt (Brodsky et al. 1996). For shear tests with higher confining pressures, Young’s modulus increases. The specific values of Young’s modulus used for the normalization process were 21, 27, and 43 GPa for confining pressures of 2.5, 5, and 10 MPa, respectively.

3.3 Dilatancy versus Consolidation

Before we discuss the influence of moisture on reconsolidation of granular salt, it is informative to compare deformation processes of intact salt and those of

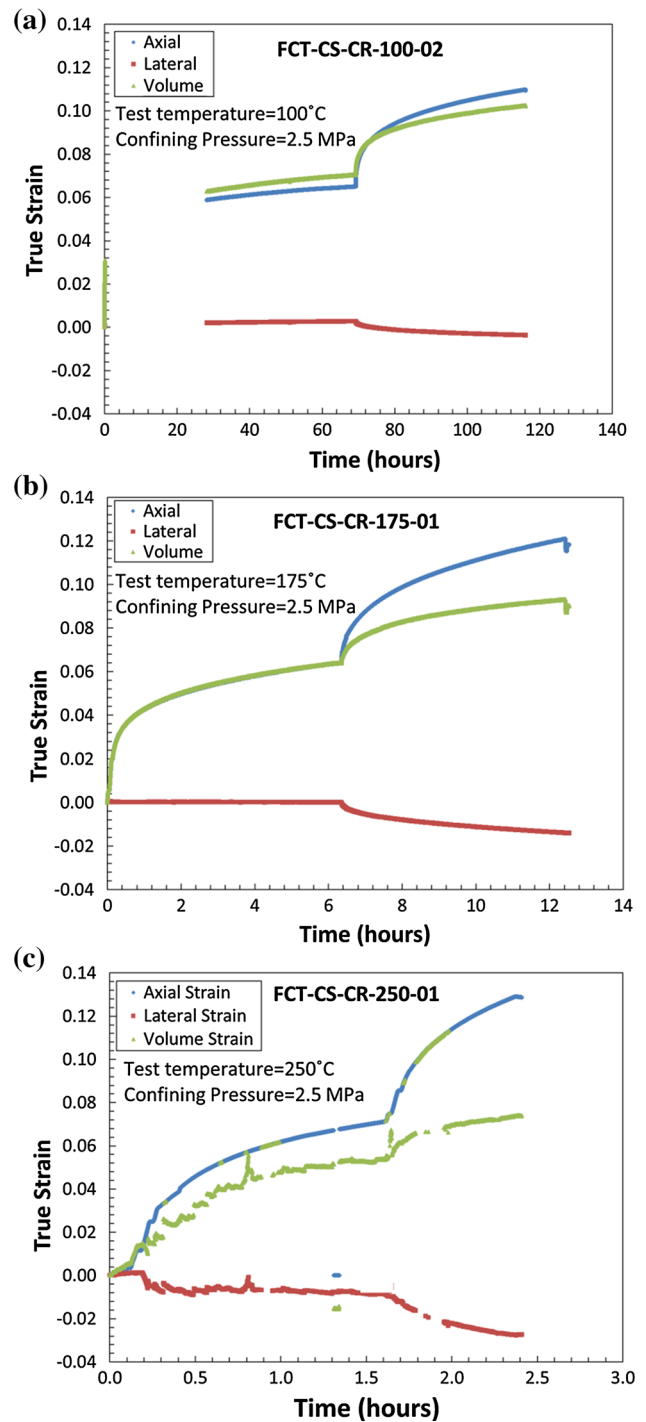


Fig. 14 True strain versus time a 100 °C, b 175 °C, and c 250 °C

reconsolidating salt. Deformation of intact samples of natural salt enjoys a long history of testing in the laboratory. By virtue of these studies the influence of stress state and temperature on deformation has been measured and governing deformational mechanisms have been documented.

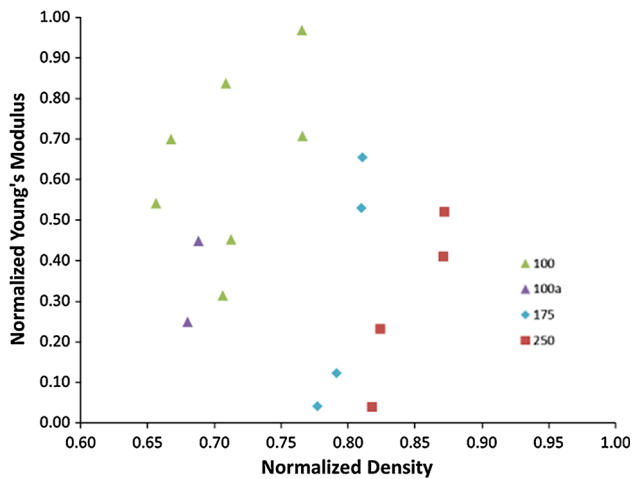


Fig. 15 Normalized density versus normalized Young's modulus

Until laboratory deformation creates damage, intact natural salt is nearly impermeable. By contrast, consolidation of granular salt starts with high porosity and high permeability and then progresses to a near intact state. Two very different phenomena and underlying deformation mechanisms are at play (Hansen et al. 2014).

Dilatant deformation of intact salt manifests by grain-boundary separation aligned parallel with the maximum principal stress. In experimentally damaged laboratory samples, a few longitudinal fractures tend to propagate and grow and accommodate the majority of the volumetric strain. These few longitudinal pathways give rise to large increases in permeability. In contrast, granular salt remains a porous medium until connectivity of pores is reduced. Sutured grain boundaries in the granular material inhibits flow even though appreciable void space remains (Hansen et al. 2014).

4 Consolidation Processes and Mechanisms

Disaggregated granular material comprises about 40 % porosity. Quasistatic consolidation processes at high porosity involve instantaneous grain rearrangement, translational sliding, rigid body rotation, and grain breakage. These predominantly mechanical processes remove void space by grain rearrangement. As porosity decreases, mechanical compaction no longer effectively reduces void space as grain-to-grain contact area increases. Further consolidation is enabled by grain-boundary processes and by dislocation motion, which accounts for grain shape changes.

This research applies to salt repositories for heat-generating nuclear waste, closure systems, and backfilling including the annulus around waste packages that take advantage of salt's exceptional properties. Reconsolidation

of granular salt is of high interest in the United States and Germany, countries actively collaborating in salt repository research, design and operation (Hansen et al. 2013). The realm of salt consolidation in this regard includes routine room backfill for structural stability, engineered systems to affect low permeability seal capability relatively quickly, and higher-temperature environments near heat-generating waste canisters. In almost all applications using crushed salt in the field, the most important characteristics are those that obtain at low porosity and attendant low permeability. Here we will emphasize reconsolidation in the sense of seal system performance; although it should be recognized that slurry placement of room backfill reconsolidates readily. In fact, all empirical evidence—natural, experimental and anthropogenic—lead to a conclusion that granular salt reconsolidates to an impermeable medium under a wide range of nominal stress and environmental conditions.

For purposes of salt repository applications and related industrial functions, micromechanical mechanisms during late stages of consolidation are the most relevant. It is well understood that brittle consolidation processes usually accompany construction practices. Dynamic compaction, for example, tends to pulverize grains during construction. A desired outcome of construction is to place geotechnical barrier material at an initial condition of low porosity, which minimizes the time between placement and functionality.

4.1 Observational Techniques

Observational approaches include optical and scanning electron microscopy. Samples are produced from both deformed and native salt, and comprise polished 5-mm thick petrographic sections, etched cleavage chips, and freshly broken surfaces. Microstructure is highlighted by etching techniques whereby the sample is agitated in a solution of methanol saturated with PbCl_2 for a few seconds and stopped by submersion in butanol.

After the samples were successfully consolidated in the laboratory experiments, they were cut in half length-wise using a low-damage diamond wire saw and subsequently quartered. A variety of subsamples were prepared for observational work. The quarter-round subsections were broken by hand to expose a surface of the compacted material, which was sputter-coated and examined by SEM. The quarter-round pieces were used to prepare for optical sections and thick-thin sections.

Identification and documentation of consolidation processes are inferred from optical and scanning electron microstructural observations as shown in the following sequence of photomicrographs. Figure 16 includes representative stages of progressive consolidation processes from high porosity to low porosity (Hansen et al. 2015).

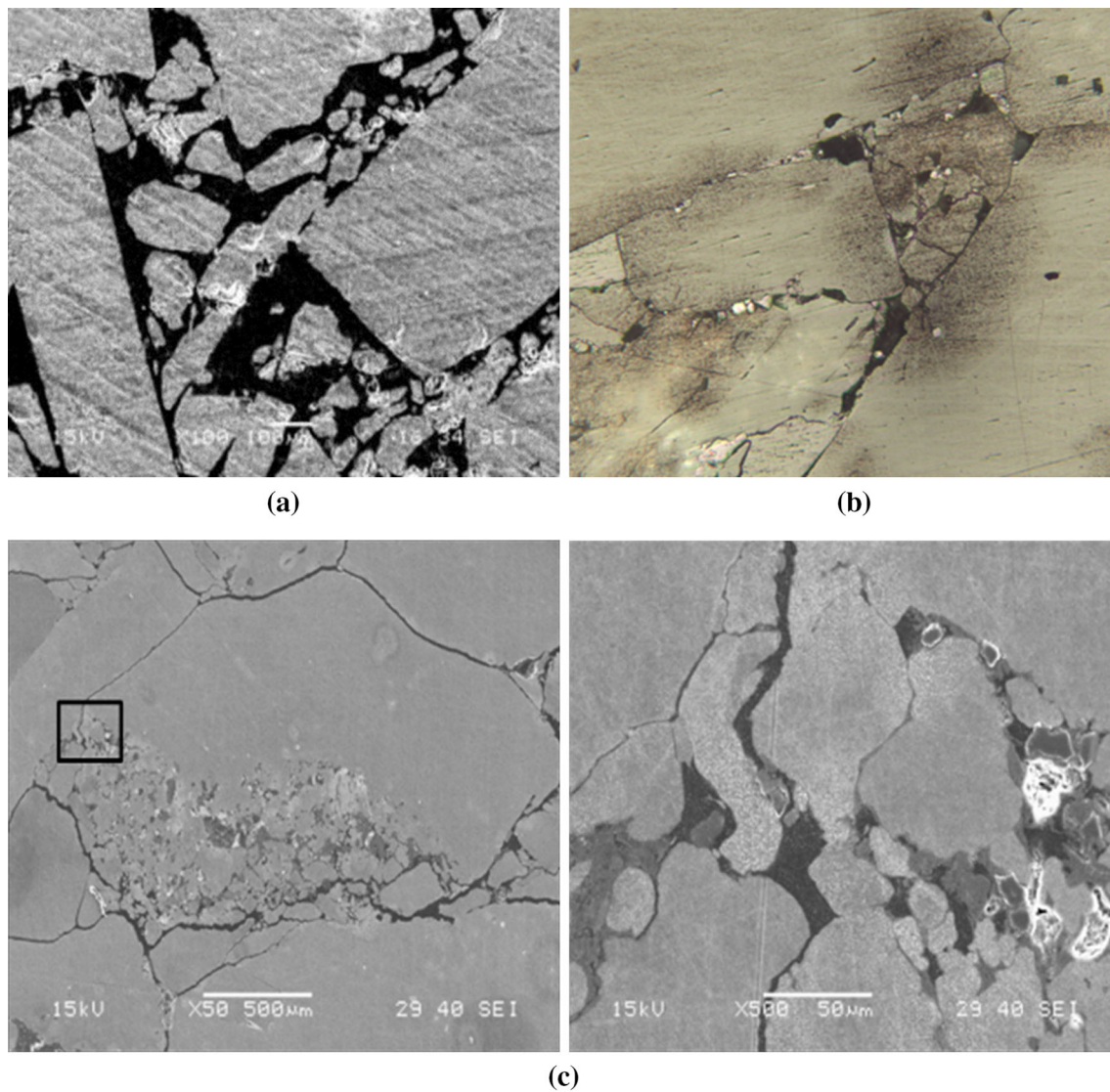


Fig. 16 Examples of consolidation processes from high (a) to low (c) porosity

Figure 16a is taken from the BAMBUS II field test (Bechthold et al. 2004) and depicts brittle cleavage fracture and translational sliding at 25 % porosity. Figure 16b is a sample from a room that was back-filled with salt slurry. The cubic habit exemplifies brittle cleavage fracture; fine particles result from pulverization along grain boundaries; well meshed grain boundaries are achieved through pressure solution. Figure 16c is taken from the thin-sectioned laboratory sample FCT-CS-SQ-250-02 that was consolidated at 250 °C to a normalized density of 0.93. It exemplifies well sutured grain boundaries in the larger view (left) and extensive plastic deformation of individual grains at higher magnification (right). We use existing documentation of consolidation mechanisms, as illustrated in Fig. 16, to guide our interpretations of the granular salt consolidation in our experiments.

4.2 Moisture Effects

Consolidation processes depend on both external and internal conditions. Variables include stress state, instantaneous porosity, deformation rate, water content, and temperature. In the setting of a salt geotechnical barrier, stress conditions are imparted by creep closure of the surrounding formation. In repository applications, most granular salt reconsolidation will occur at ambient temperature, although thermal effects will become important in some disposal situations, such as annulus backfilling around heat-generating waste canisters. As porosity diminishes an increasing number of grain surfaces are brought into contact. Spiers and Brzesowsky (1993) described effects of moisture on the contact surface under these conditions as grain-boundary diffusional pressure

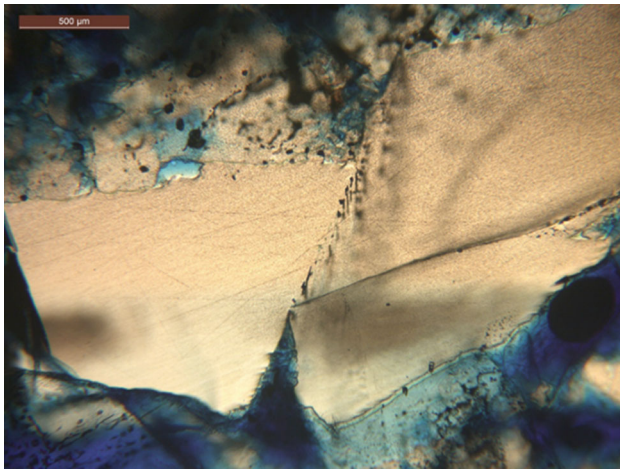


Fig. 17 Grain-boundary pressure solution processes

solution and plasticity-coupled pressure solution are set up by a diffusive flux of solutes from the contact area to the free pore surface. We observe these consolidation processes in our experimental work as shown in Fig. 17, which is an example of dislocation creep operating in concert with pressure solution processes. This photomicrograph was taken from the 5 mm-thin sectioned sample FCT-CS-HQ-ALL-01, which was consolidated to a fractional density of 97 %. The horizontal, undulatory grain-boundary on the left side of the micrograph exhibits pressure-solution and re-deposition. In the center, plasticity processes shape the grain such that the tip molds into the grain-boundary intersection; this deformation couples with pressure solution that moves mass along the boundaries as the grains fuse together. The grain-boundary is decorated with fluid

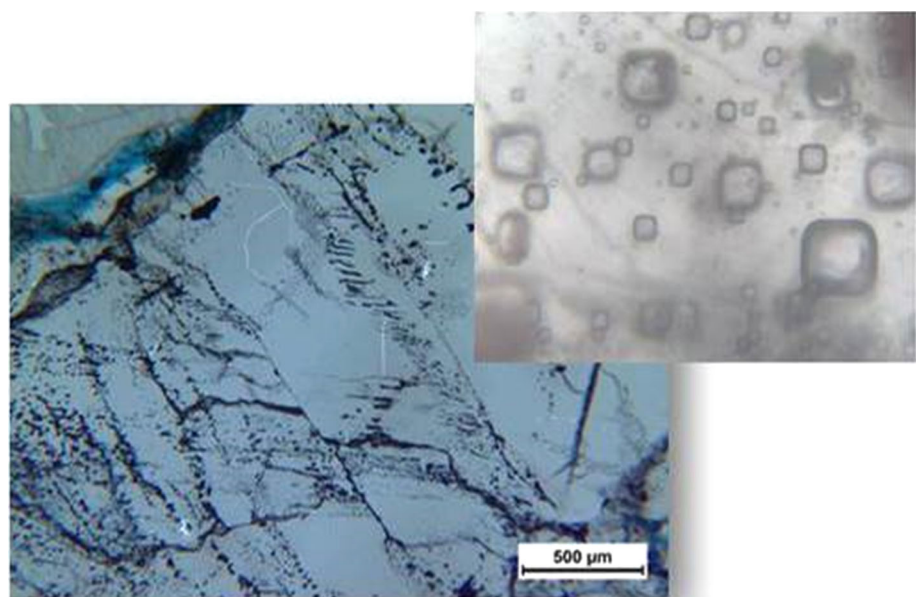
inclusions. In addition, the tightly sutured grain-boundary on the lower right benefits from alignment between grains and ready pressure solution transports outward to the right as the boundary heals (Mills et al. 2014). Note the last vestiges of cubic inclusions along the healing boundaries.

In this research as elsewhere (Hansen et al. 2015) grain distortion provides evidence of extensive dislocation creep. Individual grains exhibit internal plastic deformation, including small subgrain sizes, consistent with high stress levels. In experiments using run-of-mine salt from a bedded formation, it appears the crystal plasticity facilitates movement of internal fluid inclusions to grain boundaries whereupon pressure solution re-deposition processes actively consume smaller grains. Micromechanical processes are likely to be influenced by temperature, confining pressure, and impurities, but are most strongly dependent on the presence of sufficient water at grain boundaries to enable solution-precipitation phenomena.

4.3 Moisture Availability

A key question regarding consolidation concerns the availability of brine on grain boundaries. In the current research, a significant observation was venting of brine from the reconsolidating sample during the test. Bedded salt formations are typically interspersed with non-halite stringers, such as anhydrite interbeds, clay layers and possibly other (horizontal) discontinuities arising from the initial geologic evaporation sequences and diagenesis. Bedded salts usually contain arrays of fluid inclusions within the crystal structure as shown undeformed in the inset of Fig. 18. Estimates of total water content in bedded

Fig. 18 Lower left show trails of fluid inclusions in deforming grains from 250 °C test. *Inset* is array of undeformed fluid inclusions



salt vary between 0.1 and 0.8 weight percent [DOE, 1986]. The average water content for this WIPP salt sampling is 0.45 weight percent (Bauer et al. 2014); they measured 0.1, 0.16, and 0.25 weight per cent brine release at 100, 175, and 250 °C. Presumably a similar amount of brine was released in these experiments, and mobilized/made available to participate in the deformation. The observations below document brine presence.

The deformed crystal in Fig. 18 captures motion of internal fluid inclusions on {110} planes and tightly closed grain boundaries. The blue hue is caused by epoxy impregnation from thin sectioning. Fluid inclusions tend to collect along the tight grain boundaries, as might be expected as the fluid itself promotes healing along the grain boundary. The high degree of mobility of the inclusions can be seen in the dark lineations at an angle to the grain boundaries (presumably along {110}). These observations document cubic fluid inclusion migration to the grain boundaries by translational distortions of the crystalline structure. Based upon such observations, sufficient brine is migrated to the grain boundaries to promote fluid- assisted crystal plasticity.

Current studies use run-of-mine bedded salt from WIPP, which has been shown to contain ample moisture to support densification processes at the grain boundaries. Domal salt has been considered viable for nuclear waste disposal, as well. It is therefore informative to examine domal salt internal water content. Because of diapiric rise and multiple episodes of recrystallization domal salt has fewer impurities and much less brine in the crystal structure. However, domal salt does have brine along many grain boundaries. In Fig. 19a, b below, we capture images of grain-boundary fluid in salt from Avery Island salt dome. The total amount of fluid is minute, but brine-aided mechanisms require minuscule quantities.

The photomicrographs in Fig. 19 are taken from cleavage chips, which are nominally 2–3 mm thick. The

microscope can scan through the single crystal and focus at selected depths. Therefore, some of the image appears out-of-focus. In Fig. 19a cubic inclusions inhabit a healed volume within a single crystal. Termination of fluid inclusion zones is shown in both micrographs. Figure 19b shows vestige elongate inclusions decorating linear and non-linear healing features. Figure 19b also illuminates dendritic channels that appear to be dry.

Reconsolidation processes have been documented in laboratory experiments on natural and artificial salt aggregates, large-scale tests, and natural analogues. Empirical evidence indicates that fluid-aided processes will be operative in typical bedded salt as porosity reduces below 10 %, even if no moisture is added. Observations concerned with bedded salt show adequate moisture is available from negative crystals, grain-boundary fluid and hydrous minerals to sustain fluid-assisted processes. Nominally, domal salt contains much less moisture than bedded salt, but as shown in the micrographs in Fig. 19 above, it would appear that fluid film is largely present on grain boundaries, especially in zones of incipient healing.

4.4 Mechanisms

Consolidation processes at high porosity involve instantaneous grain rearrangement and microfracture. These processes remove void space to a point at which grain-boundary processes and crystal plastic mechanisms begin to dominate further porosity reduction. As porosity is reduced, plastic deformation is accommodated by slip along the dodecahedral {110} planes. Presented are a few photomicrographs from tests that were taken to <10 % porosity.

Crystal deformation is shown in Fig. 20, taken in transmitted light on a thick-thin section prepared from granular salt reconsolidated to low porosity at 250 °C. The blue coloration is epoxy mounting material. The black

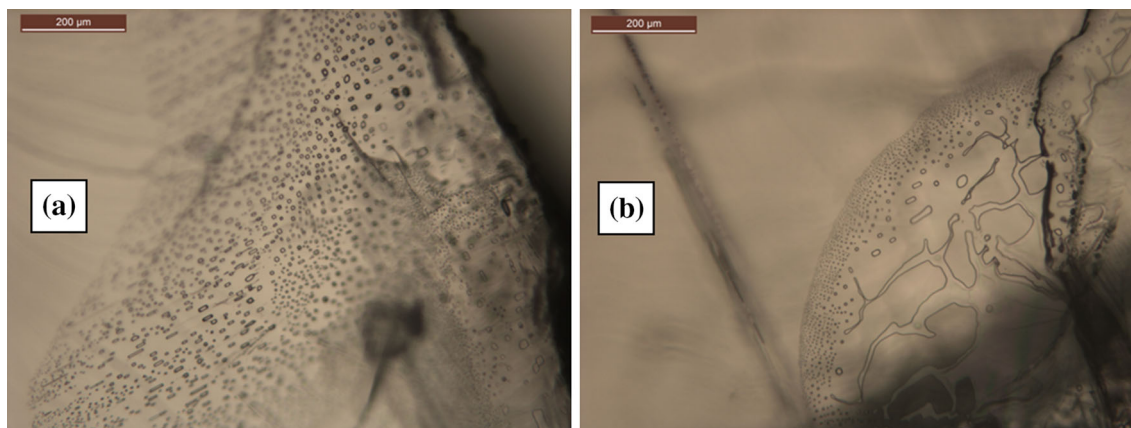


Fig. 19 a, b Grain-boundary fluid in Avery Island Salt

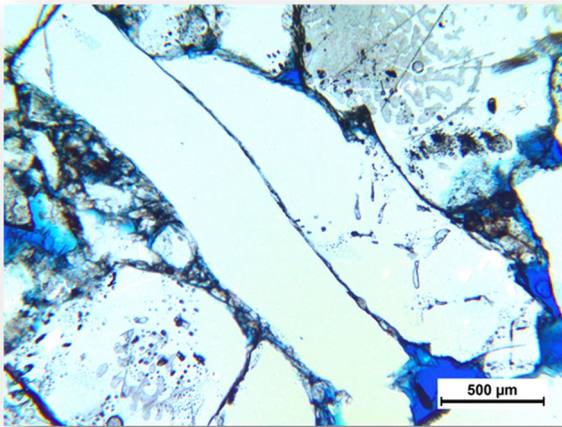


Fig. 20 Extensive grain deformation during reconsolidation at 250 °C

speckles within grains are mostly fluid inclusions. Exceptional crystal plasticity and compatible grain boundaries are exhibited between the elongate grains in the center of the frame. Compare the plentiful fluid inclusions in the relatively large equant grains in the lower left and upper right quadrants of the field of view with the absence of fluid inclusions in the paired grains that display the tight boundary and remarkable elongation. Under these conditions at low porosity the densification processes involve plasticity-coupled pressure solution (Spiers and Brzesowsky 1993).

Also portrayed in the photomicrograph in Fig. 20 are the pulverized grains clustered on the left lower area of view. All similar minute grains have been completely consumed between the two long, slender grains. Elongation facilitated by slip on {110} planes appears to have translated the ubiquitous fluid inclusion to the grain boundaries. The fluid thereby made available to the grain-boundary was sufficient for pressure solution and consumption of the particulate.

The photomicrograph in Fig. 21 is taken from a single grain extricated from FCT-CS-SQ-250-01 (see Table 2), which was consolidated at 250 °C to measured volumetric strains of 31 %. Highly distorted grains, such as these, were cleaved with some difficulty. One first notices that the cleavage plane itself is highly warped and gives the surface an undulatory fabric. The crystal structure exhibits arrays of well-developed subgrains indicative of thermally activated climb recovery. In addition, the free-dislocation density within the polygons is very low, also indicating recovery by climb.

Microscopic studies will be continued to elucidate salt substructure features at each temperature as this research continues.

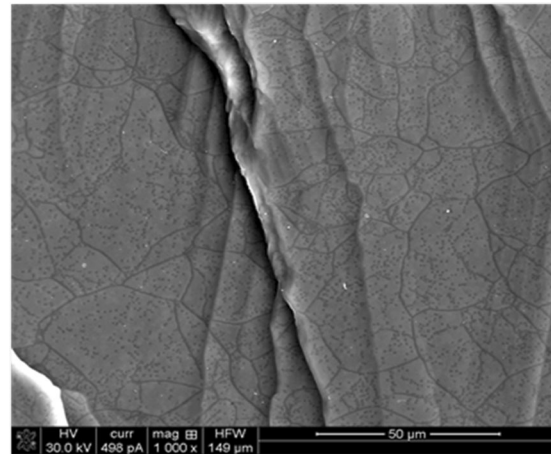


Fig. 21 Etched cleavage chips from samples consolidated at 250 °C

5 Conclusions

An experimental program was implemented to systematically evaluate crushed salt consolidation as a function of stress and temperature conditions. The laboratory studies provide consolidation behavior for temperatures to 250 °C and stresses to 20 MPa.

The test matrix includes isostatic, shear, and creep consolidation tests as a function of temperature. Limited determinations of elastic properties versus normalized density have been made. Experimental parameters were selected to acquire data for use in fitting constitutive models with a minimum number of tests, while initially exploring the desired range of temperature, pressure and stress space.

An important observation during these tests is production of brine from the pore pressure port for 250 °C tests during the heating phase when the specimen was unconfined. This observation suggests the existence of significant amounts of trapped brine (i.e., intragranular porosity), indicating ample moisture for grain-boundary consolidation processes.

Sandia National Laboratories is a multi-program laboratory managed and operated by Sandia Corporation, a wholly owned subsidiary of Lockheed Martin Corporation, for the U.S. Department of Energy's National Nuclear Security Administration under contract DE-AC04-94AL85000. SAND2015-7324J.

References

- Aubertin M, Hardy HR (1996) *The Mechanical Behavior of Salt*, Proceedings of the Fourth Conference. Montreal Canada. Trans Tech Publications (ISBN 0-87849-103-1)

- Bauer SJ, Urquhart A, Broome ST, Hansen FD (2014) Experimental Determinations of Thermophysical Properties of Reconsolidated Crushed Salt ARMA 14-144. Sandia National Laboratories, Albuquerque
- Bechthold W, Smailos E, Heusermann S, Bollingerfehr W, Sabet B, Rothfuchs T, Kamlot P, Grupa J, Olivella S, Hansen F (2004) Backfilling and sealing of underground repositories for radioactive waste in salt (BAMBUS II Project): Final Report. EUR 20621 EN. European Commission. Directorate General for Research. Office for Official Publications of the European Communities
- Brodsky NS, Hansen FD, Pfeifle TW (1996) Properties of Dynamically Compacted WIPP Salt. Proceeding of the 4th Conference on the Mechanical Behavior of Salt, Trans Tech Publications, Clausthal-Zellerfeld, Germany. SAND96-0838C
- Callahan GD (1999) Crushed salt constitutive model, SAND98-2680. Sandia National Laboratories, Albuquerque
- Department of Energy (1986) Environmental Assessment of Deaf Smith County, Texas
- Hansen FD, Leigh CD (2011) Salt Disposal of Heat-generating Nuclear Waste, SAND2011-0161. Sandia National Laboratories, Albuquerque
- Hansen FD, Steininger W, Biurrun E (2013) Proceedings of the 4th US/German Workshop on Salt Repository Research, Design, and Operation. Prepared for U.S. Department of Energy Used Fuel Disposition Campaign FCRD-UFD-2014-000335. SAND2013-10592P. Sandia National Laboratories. Albuquerque, New Mexico
- Hansen FD, Popp T, Wieczorek K, Stührenberg D (2014) Salt reconsolidation principles and applications. Nuclear Energy Agency Report. SAND2014-4502P. Sandia National Laboratories, Albuquerque
- Hansen FD, Popp T, Wieczorek K, Stührenberg D (2015) Salt reconsolidation applied to repository seals. Proceedings of the Eighth Conference on the Mechanical Behavior of Salt. SAND2014-19950 C. Sandia National Laboratories, Albuquerque
- Mills M, Hansen F, Bauer S, Stormont J (2014) Microstructural Observations of Reconsolidated Granular Salt. AGU Abstract, San Francisco
- Spiers CJ, Brzesowsky RH (1993) Densification behaviour of wet granular salt: theory versus experiment. 7th Symposium on Salt. Vol. I. Elsevier Science Publishers B.V. Amsterdam
- Wallner M, Lux K-H, Minkley W, Hardy HR (2007) The mechanical behavior of salt, Proceeding of the Sixth Conference. Hannover Germany. Balkema. ISBN 13: 978-415-444398-2